Friction

Research Article

Cr doping modification for tribological behavior of Cr/a-C multilayer coatings against PEEK under diverse operational conditions

Xiaohui Zhou[1,3], Yingpeng Zhang[1], Hao Li[1], Li Cui[1], Wei Yang[1], Aiying Wang[1,2], Peng Guo[1,✉], Peiling Ke[1,2,✉]

Cite this article: Zhou X, Zhang Y, Li H, et al. *Friction*, 2025, **13**: 9440920. https://doi.org/10.26599/FRICT.2025.9440920

ABSTRACT: Considering the increasing demand for wear-resistant materials used for various frictions with dynamic sealing parts, we employed hybrid magnetron sputtering technology to fabricate Cr/amorphous carbon (a-C) multilayered coatings with and without Cr doping for comparison. The tribological behaviors of coatings paired with polyether ether ketone (PEEK) balls were investigated under different friction environments, including an evolving atmosphere, a NaCl solution, polyalphaolefin (PAO) oil, and water-in-oil (W/O). The results demonstrated that the tribological properties of all friction pairs were strongly influenced by the surrounding environment. In the atmosphere and in a NaCl solution, the addition of Cr promoted the formation of a-C-containing transfer films, thereby yielding stable and low friction characteristics. However, the dominant factor contributing to the tribological performance shifted from the coatings themselves to the PAO oil film with PAO medium. In the case of the W/O solution, both the facile reactivity of Cr and the intrinsic instability of the W/O mixture accelerated the presence of Cr_2O_3, which caused more severe wear. The current observations not only identified the tribological failure mechanism of Cr/a-C coatings with and without Cr doping modifications in conjunction with their PEEK counterparts but also addressed the importance of designing and fabricating adaptive lubricant coatings for harsh multi-environment applications.

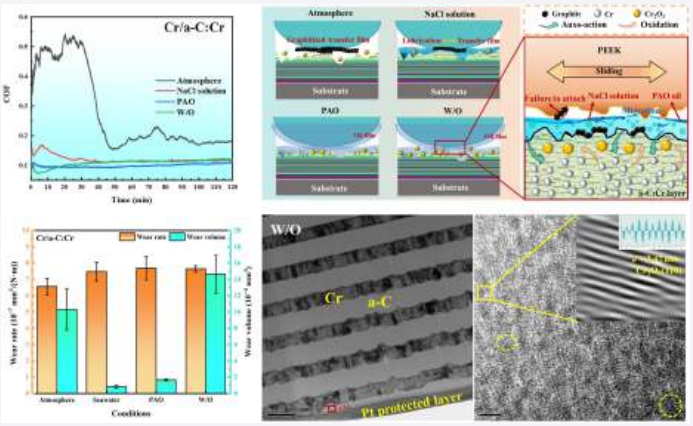

KEYWORDS: polyether ether ketone (PEEK); amorphous carbon; polyalphaolefin (PAO) oil; dynamic sealing; tribo-chemistry

1 Introduction

The art of sealing is an essential craft, vital for guaranteeing the security, dependability, and enduringness of a mechanical apparatus. Its domain stretches far and wide, encompassing not only the automotive and aerospace industries but also the realms of petroleum, chemistry, and beyond. Sealing occupies a paramount position in the advancement of industrial innovation [1, 2]. Polyether ether ketone (PEEK) and stainless steel are frequently utilized as auxiliary materials for dynamic sealing owing to their condensed composition, commendable self-lubricating capabilities, and cost-effectiveness in processing [3, 4]. While certain marine engineering equipment, such as plunger-type seawater pumps, may encounter significant wear and endure high hydrostatic pressure, reaching an impressive 60 MPa [5, 6], the subsequent infiltration of seawater is capable of inducing alterations in lubricating conditions. This critical factor becomes the primary catalyst behind the failure and subsequent leakage of dynamic seal components [7, 8].

Amorphous carbon (a-C) coating is a solid lubricating coating with both graphite (sp^2) and diamond (sp^3) structures. It also has several distinct advantages, such as high hardness [9], excellent wear resistance [10, 11] and chemical inertness [12], so modifying its metallic counterpart with a-C has been confirmed as an effective strategy to improve the service performance of PEEK/stainless steel pairs under single lubricating conditions. For example, Jacobs et al. [13] prepared tungsten doped a-C on 100Cr6 bearing steel and found that the wear rate of the PEEK counter body was reduced by 2 orders of magnitude under dry friction and water lubrication conditions. Franta et al. [14] used

[1] Key Laboratory of Advanced Marine Materials, Ningbo Institute of Materials Technology and Engineering, Chinese Academy of Sciences, Ningbo 315201, China. [2] Center of Materials Science and Optoelectronics Engineering, University of Chinese Academy of Sciences, Beijing 100049, China. [3] School of Physical Science and Technology, ShanghaiTech University, Shanghai 201210, China.

✉ Corresponding authors. E-mail: P. Guo, guopeng@nimte.ac.cn; P. Ke, Kepl@nimte.ac.cn

Received: December 27, 2023; Revised: March 13, 2024; Accepted: April 20, 2024

© The Author(s) 2025. This is an open access article under the terms of the Creative Commons Attribution 4.0 International License (CC BY 4.0, http://creativecommons.org/licenses/by/4.0/).

a-C modified Ti6Al4V alloy to significantly increase the service life of PEEK bearing sleeves in saline physiological solution (9 g/L NaCl).

Considering that interfacial chemical reactions occur under varying medium conditions, it is worth noting that the utilization of a-C may unfavorably impact the wear resistance of PEEK. Patnaik and co-workers [15] pointed out that the PEEK counter body suffered severe wear against Ag-doped Cr/a-C under physiological fluid lubrication, and the scattered particles of PEEK in the sliding interface resulted in a long run-in process. Escudeiro's team [16] found that, for a-C coated Ti-alloys and PEEK pairs, the a-C coatings delaminated during tribological tests in bovine serum lubricant due to the synergetic effect between stress-induced corrosion and cyclic fatigue at the interface.

Clearly, the a-C coated metal and PEEK pairs exhibit an obvious environmental-dependent tribological behaviors. In our previous work, the inherent graphitization of the a-C layer and suppressed adhesive reaction of the transferred chromium (Cr) layer were confirmed to improve the lubrication performance of the a-C/PEEK pair [17]. In addition, due to the solid lubrication provided by the metal, a large number of studies have shown that Cr doping can significantly improve the wear resistance of a-C under dry sliding conditions [18, 19]. However, in the realm of liquid lubrication, the impact of incorporating Cr as a dopant could deviate from the anticipated outcomes.

Previous research revealed that a multilayered structure composed of Cr and a-C has the potential to alleviate residual stress, thwart corrosion pathways, and increase the tribo-corrosion resistance of coatings [12, 20]. Therefore, in this work, Cr/a-C and Cr-doped Cr/a-C (Cr/a-C:Cr) multilayered coatings were prepared on mirror-polished 17-PH stainless steel by multi-target magnetron sputtering. The tribological behavior of the two coatings against PEEK balls was studied by a pin-on-desk reciprocating tribometer. Three lubricants, namely, polyalphaolefin (PAO) base oil, 3.5 wt% NaCl solution, and water-in-oil (W/O), were used to simulate the multiple operating conditions for dynamic seal components in deep-sea hydraulic technology. The interfacial structure evolution and tribo-chemistry were investigated, and the related failure mechanism was also discussed.

2 Materials and methods

2.1 Coating preparation

The Cr/a-C and Cr/a-C:Cr multilayered coatings were deposited by a self-developed direct current magnetron sputtering (DCMS) system consisting of a graphite target (purity: 99.99 wt%) and a chromium target (purity: 99.99 wt%) with the same dimensions of 380 mm × 100 mm × 7 mm. Mirror-polished 17-PH stainless steel with a size of ϕ17 mm × 3 mm was used as the substrate. The arithmetic mean roughness (R_a) of the substrate was 5.22 nm, and the three-dimensional (3D) structure diagram of its surface is shown in Fig. S1(a) in the Electronic Supplementary Material (ESM).

Prior to deposition, the substrates were ultrasonically cleaned with acetone and anhydrous ethanol for 10 min and subsequently mounted on a rotation holder 15 cm from each target. When the base pressure of the chamber was evacuated to 4×10^{-5} Torr, the substrates were etched by discharged Ar^+ from a linear ion source to remove contaminants on the substrate surface, with a DC pulsed bias of −200 V. Thereafter, a combination of ($Cr+Cr_xN$) layers was deposited on the substrate by the sequential ionization of the Cr target in Ar and $Ar+N_2$ gases to enhance the interfacial adhesion strength. The Cr buffer layer was deposited on the substrate with a target power of 1.8 kW and a bias voltage of −100 V. In the subsequent deposition of the Cr_xN layer, the N_2 flow was 20 standard cubic centimeters per minute (sccm). Then, during the deposition of the a-C layer, the graphite target power was 2.0 kW, and the bias voltage was −200 V. When depositing the Cr layer, it is essential to deactivate the power supply to the graphite target and rotate the substrate so that it is aligned with the Cr target. Conversely, when depositing the a-C layer, the power supply to the Cr target must be switched off, and the substrate rotates to face the C target. The intermittent a-C and Cr layers were deposited in turn 7 times, and the thickness of each layer was controlled at ~107 nm.

Finally, the top-most a-C and Cr-doped a-C layers with a thickness of 300 nm were deposited. The Cr target was 0.1 kW, and the graphite target was 2.0 kW for depositing the a-C:Cr top layer. The total thicknesses of the Cr/a-C and Cr/a-C:Cr multilayered coatings were ~2.0 and ~2.2 μm, respectively. Figure 1 shows schematic diagrams of the Cr/a-C and Cr/a-C:Cr multilayered coatings.

2.2 Characterization method

The cross-sectional morphologies and microstructures of the deposited coatings and the wear tracks after tribological testing were studied via a transmission electron microscope (TEM; Talos F200X, FEI, USA), and the samples were prepared via focused ion beam technology (FIB; Auriga, Carl Zeiss, Germany). The electron energy loss spectrum (EELS) was used to obtain the sp^2 fraction of the a-C layer. The surface roughness of the substrate and the PEEK ball was measured by an atomic force microscope (AFM; Dimension 3100, Vecco, USA) with a measuring range of 10 μm × 10 μm.

The surface wettability of the PEEK, Cr/a-C, and Cr/a-C:Cr coatings was measured with a dynamic contact angle measuring

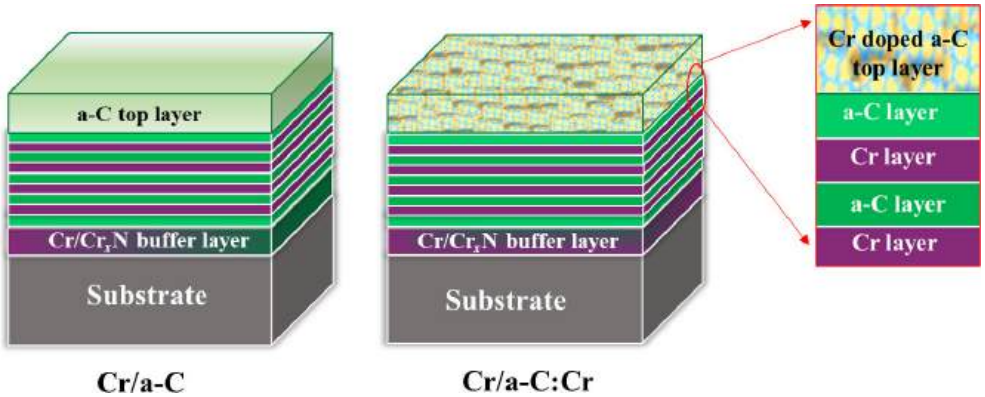

Fig. 1 Schematic diagrams of Cr/a-C and Cr/a-C:Cr multilayered coatings.

instrument (DCAT21, Dataphysics, Germany). The test drops were deionized water and 3.5 wt% NaCl solution, and the volume of the dropped liquid was 3 μL.

The hardness (H) and elastic modulus (E) of the coatings were tested by a nanoindenter (G200, MTS Agilent, USA) with a Bruker diamond indenter, and the continuous stiffness method was used. For each sample, the indentation depth was 300 nm. To determine the influence of the substrate, H and E were calculated within a depth of 200 nm, and each sample was measured at least 6 times.

The surface morphologies of the wear tracks were observed using a scanning electron microscope (SEM; Quanta FEG 250, FEI, USA) equipped with an energy dispersive spectrometer (EDS). The wear scars of PEEK were characterized by an optical microscope (Axio Imager 2, Zeiss, Germany). The composition and atomic binding state of the coatings were detected by an X-ray photoelectron spectroscope (XPS; Axis Ultra DLD, Kratos Analytical, UK). The microstructure and atomic bonding of the coatings before and after tribological tests were investigated by an confocal micro-Raman spectroscope (inVia Reflex, Renishaw, UK; 532 nm).

2.3 Tribological tests

The tribological tests were performed by a linear reciprocating tribometer (MFT5000, Rtec, USA). For comparison with other research endeavors [21], the applied normal load, frequency, and length were 5 N, 2 Hz, and 5 mm, respectively, and the counterbody was a 6 mm diameter PEEK ball. The R_a of PEEK was 13.8 nm, and the 3D structure diagram of its surface is shown in Fig. S1(b) in the ESM. The corresponding maximum contact stress (σ_{max}) was 114.8 MPa. The calculation of the contact stress can be obtained elsewhere [22].

Initially, the samples were securely positioned within custom-made fixtures utilizing screws, with the fixtures segregated into distinct upper and lower tiers with dimensions of 130 mm × 100 mm × 25 mm. The upper tier was intricately fashioned with recesses, delving to a depth of 22 mm, to accommodate the lubricant. The lubricant was added to fully immerse the sample, thereby commencing the friction test. A visual representation of the apparatus can be found in our prior work [17]. The lubricants used were 3.5 wt% NaCl saline solution, PAO oil, and water-in-oil (W/O). The kinematic viscosity of PAO was 19 mm^2/s [23]. For the W/O lubricants, the water content was 9.1 wt%. Phacoemulsification was performed for 10 min before the addition of the W/O lubricant.

After the tribological tests, a three-dimensional optical profiler (TE, UP-Lambda, USA) was used to observe the morphology of the wear tracks on the coatings and the wear scars on the PEEK counterparts. The formulas for calculating the wear rate of coatings and wear volume of PEEK balls can be found elsewhere [17, 24].

3 Results

3.1 Cross-sectional morphologies of coatings

Figure 2 shows cross-sectional TEM images and corresponding selected area electron diffraction (SAED) patterns of the Cr/a-C:Cr

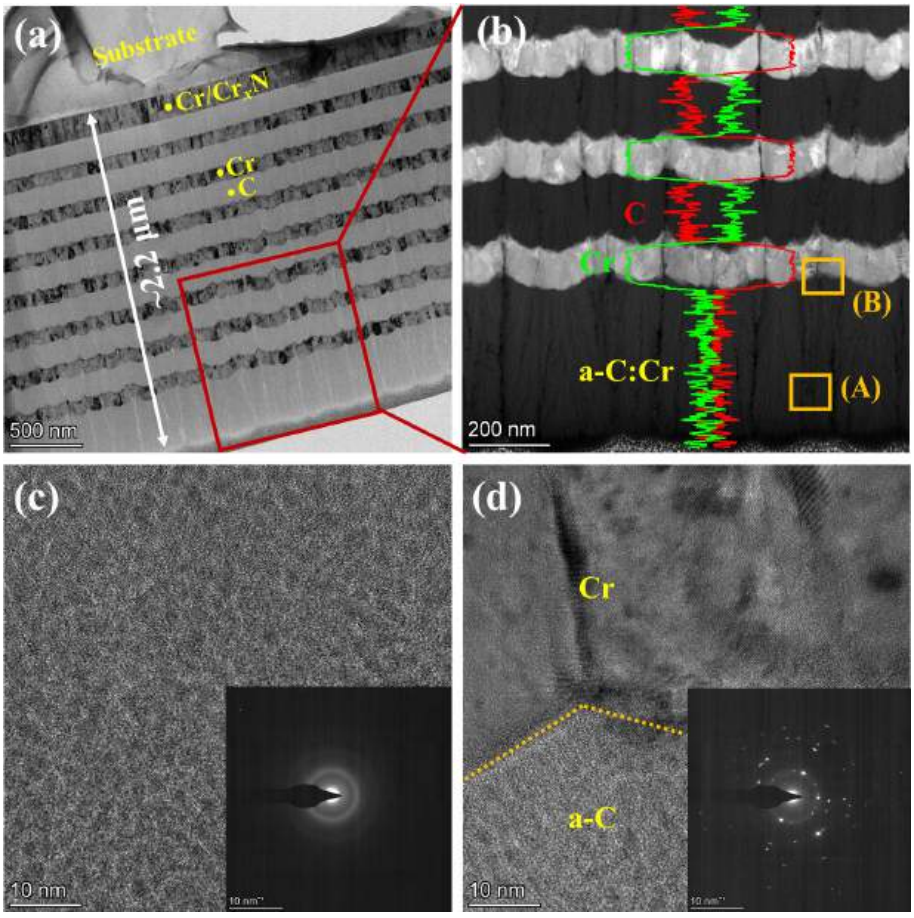

Fig. 2 Cross-sectional TEM images of Cr/a-C:Cr coating at (a) low magnification and (b) high magnification, corresponding HRTEM and SAED images of (c) a-C:Cr layer (position A in (b)) and (d) interface (position B in (b)) between a-C and Cr layers.

coating. the total thickness of the coating was approximately 2.2 μm, and the Cr layer and the C layer were alternately deposited (Fig. 2(a)). The elemental scanning distribution map showed that the content of Cr in the top layer increased compared with that in the middle a-C layer (Fig. 2(b)), and the Cr content of the top layer was approximately 2.45 at%. High-resolution TEM (HRTEM) images and SAED of the a-C:Cr layer confirmed its amorphous characteristic, and no crystalline phase was formed, as shown in Fig. 2(c). As shown in Fig. 2(d), a serration-shaped boundary was formed between the Cr layer and the a-C layer due to its typical columnar grain growth characteristics [25]. The Cr/a-C multilayered coatings had similar cross-sectional morphologies, as reported in our previous work [17].

3.2 Wettability and mechanical properties

The wetting characteristics of the solid surface play a crucial role in determining the formation of the lubricating film, subsequently influencing the frictional properties of the interface [26]. Consequently, we measured the contact angles of 3.5 wt% NaCl solution and PAO oil on PEEK, Cr/a-C, and Cr/a-C:Cr surfaces, as depicted in Fig. 3. The average contact angles of PEEK with PAO and NaCl solution were 8.5° and 90.6°, respectively. Those of Cr/a-C multilayer coatings were 16.7° and 79.8°, and for Cr/a-C:Cr coatings, the angles were 16.9° and 86.2°. PEEK and a-C coatings are lipophilic and hydrophobic due to the presence of many nonpolar molecules on their surfaces [27, 28]. The large number of hydrophobic groups, such as ethers, on the surface made PEEK more lipophilic. In addition, the doping of Cr did not change the wettability of the coating.

The H and E values of the coatings at different depths are shown in Fig. 4. The mean H and E of the Cr/a-C coating were approximately 16 and 225 GPa, respectively, while those of the Cr/a-C:Cr coating were approximately 17 and 230 GPa, respectively. This indicated that the small amount of metal doping did not significantly affect the mechanical properties of the coating. The EELS profiles of the two coatings showed that Cr doping did not affect the sp^2 content of a-C (as shown in Fig. S2 in the ESM), because its mechanical properties were mainly attributed to the amorphous carbon matrix rather than carbide crystallites at low concentrations of doping [29].

3.3 Tribological performance

In the atmospheric environment, the coefficient of friction (COF) of the Cr/a-C coating paired with PEEK was as high as 0.4, and it did not reach stability for 2 h (Fig. 5(a)). When the Cr/a-C:Cr coating was paired with PEEK, the running period was shortened to 50 min, and the COF value was stable at ~0.2 (Fig. 5(b)). It was possible that Cr inhibited the adhesion chemical reaction and accelerated the graphitization process of the coating [17]. In contrast, in the PAO oil, both pairs had the lowest COFs, ~0.08 and ~0.10, respectively. When testing under NaCl solution and water-in-oil conditions, the COFs of the two pairs increased slightly compared with that of PAO.

The wear rate of the Cr/a-C coating and the wear volume of the PEEK counterpart under different conditions are shown in Fig. 6(a). Overall, the Cr/a-C coating showed a low wear rate under all experimental conditions. Under atmospheric and NaCl solution conditions, the wear rates were relatively higher, at 5.38×10^{-7} and 5.00×10^{-7} $mm^3/(N\cdot m)$, respectively. The wear rates under PAO and W/O were 0.96×10^{-7} and 2.69×10^{-7} $mm^3/(N\cdot m)$, respectively. The cross-sectional profiles of the wear tracks on the Cr/a-C coatings are shown in Fig. S3(a) in the ESM. The wear volumes of the corresponding PEEK samples were similar, at 14.52×10^{-4}, 15.13×10^{-4}, 8.82×10^{-4}, and 11.87×10^{-4} mm^3, respectively. Since the kinematic viscosity of PAO is greater than those of W/O and NaCl solutions, the contact angle with PEEK was extremely low (Fig. 3). The PAO oil film easily formed on the PEEK surface and was not easily damaged by shear during sliding, resulting in both the lowest wear rate and wear volume.

When the Cr/a-C:Cr coating slid against PEEK, the wear rates and wear volumes exhibited completely different characteristics (Fig. 6(b)). Under atmospheric, NaCl solution, PAO, and W/O conditions, the wear rates of the coatings were low and similar, approximately 6.56×10^{-7}, 7.48×10^{-7}, 7.68×10^{-7}, and 7.64×10^{-7} $mm^3/(N\cdot m)$, respectively, which were higher than those of the Cr/a-C coating under the same conditions. The cross-sectional profiles of the wear tracks on the Cr/a-C:Cr coatings are shown in Fig. S3(b) in the ESM. The corresponding PEEK wear volumes changed greatly and were 10.34×10^{-4}, 0.83×10^{-4}, 1.66×10^{-4}, and 14.65×10^{-4} mm^3, respectively. In addition, the Cr/a-C:Cr and PEEK pairs exhibited the worst wear resistance in the W/O environment.

3.4 Investigation on the wear scar

Figure 7 shows the surface morphology of the wear scar on the PEEK ball. For the Cr/a-C coating and PEEK pair, the wear scars were larger and smoother. There was almost no accumulation of wear debris or transfer materials. For the Cr/a-C:Cr coating and PEEK pair, obvious transfer materials were observed under both atmospheric and NaCl solution conditions. The Raman spectrum of the transfer material showed obvious D and G peaks (Fig. 8), which proved that the transfer material was a graphitized film

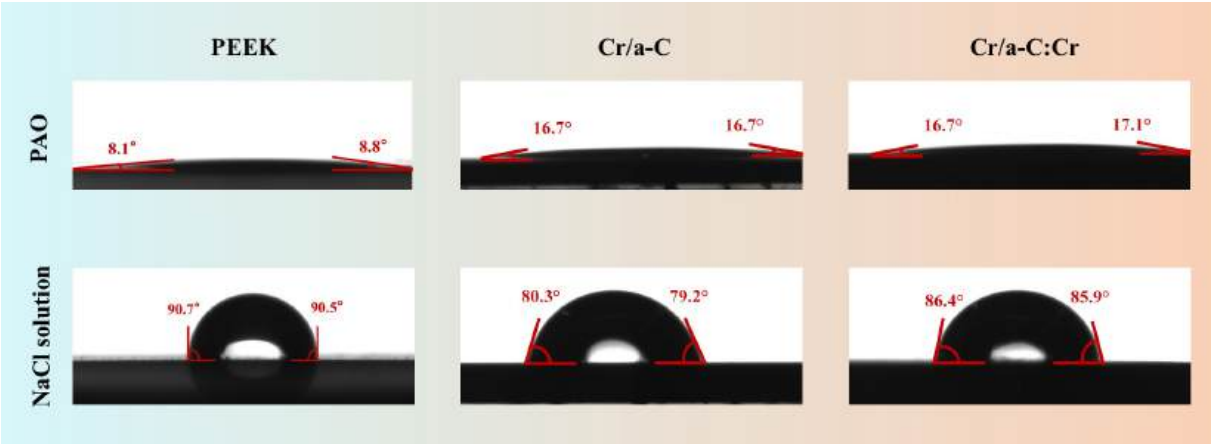

Fig. 3 Contact angles of NaCl solution and PAO on PEEK, Cr/a-C, and Cr/a-C:Cr coating.

from the a-C coating. For PAO and W/O, no Raman characteristic peak was detected under the test conditions, which was similar to the results of the original PEEK, indicating that no graphitized transfer film was formed (as shown in Fig. S4 in the ESM).

3.5 Investigation on the wear track

Raman spectroscopy was used to characterize the carbon bond structure of the two coatings before and after sliding, and the results are shown in Fig. S5 in the ESM and Table 1. For the Cr/a-C coating and PEEK pair, the G peak position and the ratio of the area of the G peak and D peak (I_D/I_G) from the wear track both increased, which indicated that the sp^2 content and cluster size increased and that graphitization of the coating occurred [30, 31]. When the Cr/a-C:Cr coating was sliding against PEEK, the changes in the G peak position and I_D/I_G were more significant. In an atmospheric environment, the G peak position changed from 1,553.56 cm^{-1} for the as-deposited sample to 1,573.72 cm^{-1}, and the I_D/I_G ratio changed from 3.45 to 4.40. In a NaCl solution, the G peak position and I_D/I_G were 1,574.35 cm^{-1} and 4.08, respectively. This showed that the doping of Cr promoted graphitization of the coating during friction. In addition, the full width at half maximum of the G peak (G_{FWHM}) was significantly lower, which indicated that the distortion of the outermost a-C layer was smaller [32, 33].

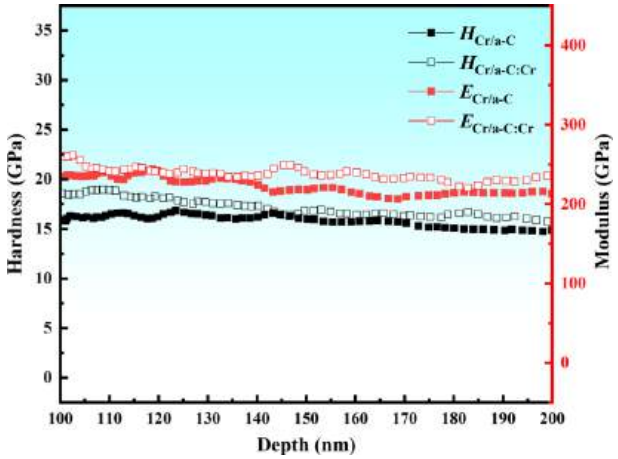

Fig. 4 Hardness and elastic modulus values of Cr/a-C and Cr/a-C:Cr coatings.

Considering the high chemical inertness of a-C and PEEK, the incorporated Cr atoms should play a more important role in the sliding interface, transfer film, and tribological behavior, so the following analysis focused mainly on the Cr/a-C:Cr coating and PEEK pair.

SEM was used to observe the morphology of the wear track of the Cr/a-C:Cr coating, as shown in Fig. 9. Under four conditions, there were a large number of micrometer-scale plows on the surface, which indicated that the coating underwent severe abrasive wear. Under atmospheric conditions, the wear track was the widest, with a size of 428.6 μm, and many abrasive grains were observed. According to the EDS results in Fig. 9(a3), the abrasive grains mainly contained O and Cr. Under NaCl solution, the wear track was the narrowest, with a size of 242.9 μm, and some particles, which were dry salt particles, appeared on its surface (Fig. S6 in the ESM). Under PAO and W/O conditions, the wear tracks had similar widths and morphologies, and they had the largest number of plows, indicating the most severe abrasive wear.

Figure 10 shows the XPS spectra of the wear track and the percentages of C 1s and Cr 2p. For Cr $2p_{3/2}$, the XPS peaks of Cr, CrO_2, Cr_2O_3 and $Cr(OH)_3$ can be fitted with binding energies of

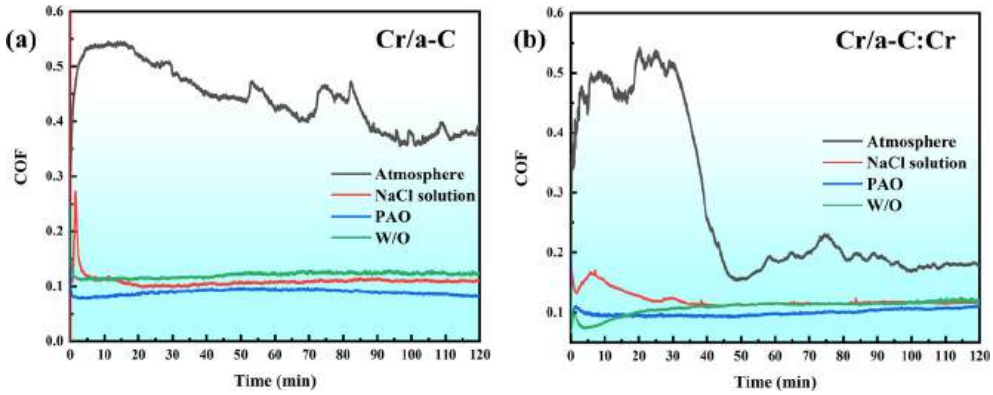

Fig. 5 COF–time curves of (a) Cr/a-C coating and (b) Cr/a-C:Cr coating against PEEK ball under different conditions.

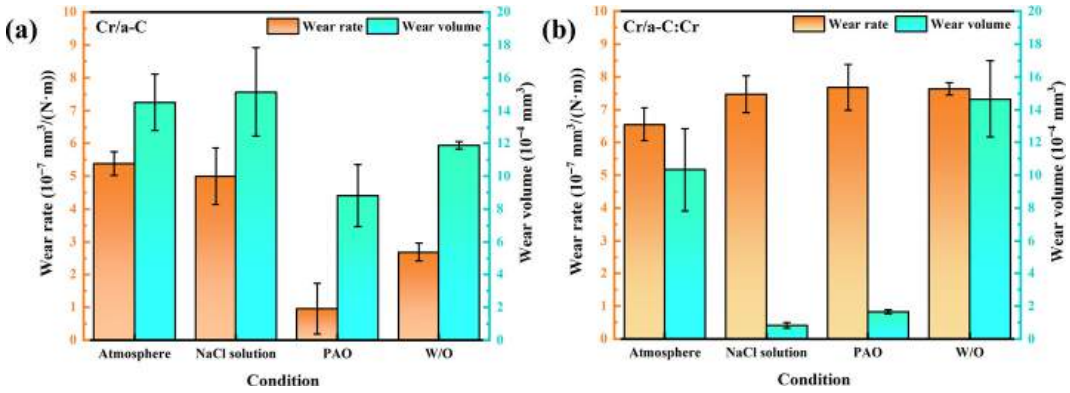

Fig. 6 Wear rates of (a) Cr/a-C coating and (b) Cr/a-C:Cr coating and wear volumes of corresponding PEEK under different conditions.

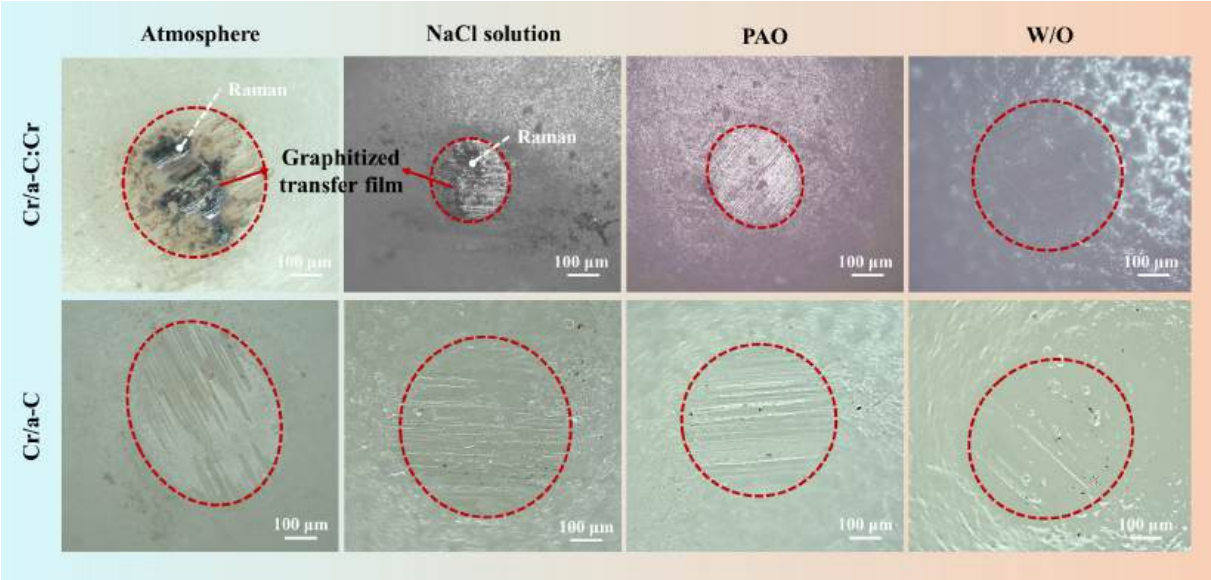

Fig. 7 OM images of wear scars on PEEK balls under different conditions.

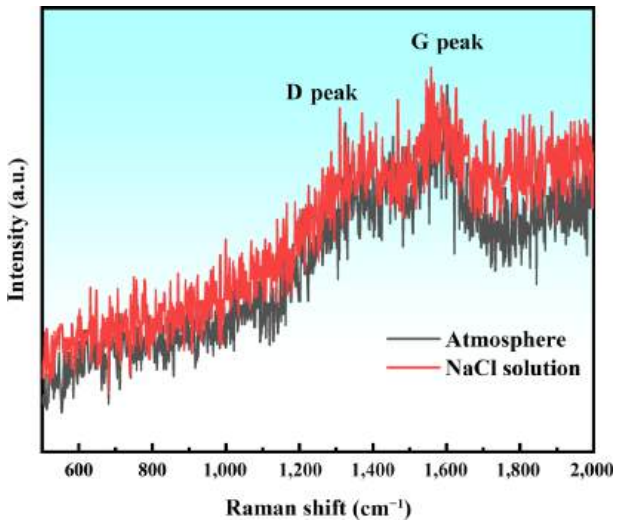

Fig. 8 Raman spectra of transfer materials at wear scar.

574.3, 576.3, 576.8, and 578.3 eV, respectively [34] (Fig. 10(a)). Under different conditions, the amount of Cr oxides varied (Fig. 10(b)), which corresponds to the results shown in Fig. 9(a3). Among them, the oxidation degree of the W/O condition was the highest, and Cr only accounted for 24%, which resulted in severe abrasive wear of the pair. For C 1s, the XPS peaks of C–C, Cr–C, C–O, and O–C=O can be fitted with binding energies of 284.6, 283, 286.5, and 288.6 eV, respectively [35, 36]. Under PAO and W/O conditions, the oxidation degree of C and the content of Cr–C bonds slightly decreased, which may be related to the oxidation of Cr and the removal of friction products during the sliding process, as shown in Fig. 10(d).

Obviously, the Cr/a-C:Cr coating exhibited the highest oxidation degree of Cr under W/O conditions. Therefore, further cross-sectional TEM observation was performed on the wear track, as shown in Fig. 11. As shown in Fig. 11(a), the Cr/a-C:Cr coating still had a compact and multilayered structure, and only the outermost a-C:Cr layer and the closely connected Cr layer showed significant wear. From the near surface of the wear track in Fig. 11(b), Cr_2O_3 nanocrystals with a size of 3–5 nm were dispersed in the a-C matrix.

4 Discussion

To understand the tribological behavior of a-C coatings and PEEK pairs in different environments, at least three factors, namely, the tribo-chemical products, the transfer film, and the interaction between the solid surface and liquid lubrication, should be considered.

For the Cr/a-C coating and PEEK pair, the COF and wear rate were greater under atmospheric conditions. After the addition of lubricant, the COF decreased to ~0.1 in all cases (Fig. 5(a)). Under PAO oil conditions, the coating and PEEK had the best wear

Table 1 Raman results of Cr/a-C and Cr/a-C:Cr coating surfaces after sliding under different conditions

Coating	Condition	I_D/I_G	G peak position (cm^{-1})	G_{FWHM} (cm^{-1})
Cr/a-C	As-deposited	2.84	1,551.15	180.72
	Atmosphere	3.03	1,549.96	177.91
	NaCl solution	3.54	1,560.05	142.44
	PAO	4.46	1,555.69	148.21
	W/O	3.92	1,549.84	161.31
Cr/a-C:Cr	As-deposited	3.45	1,553.56	159.41
	Atmosphere	4.40	1,573.72	107.79
	NaCl solution	4.08	1,574.35	149.53
	PAO	3.46	1,586.02	127.83
	W/O	3.98	1,568.31	150.84

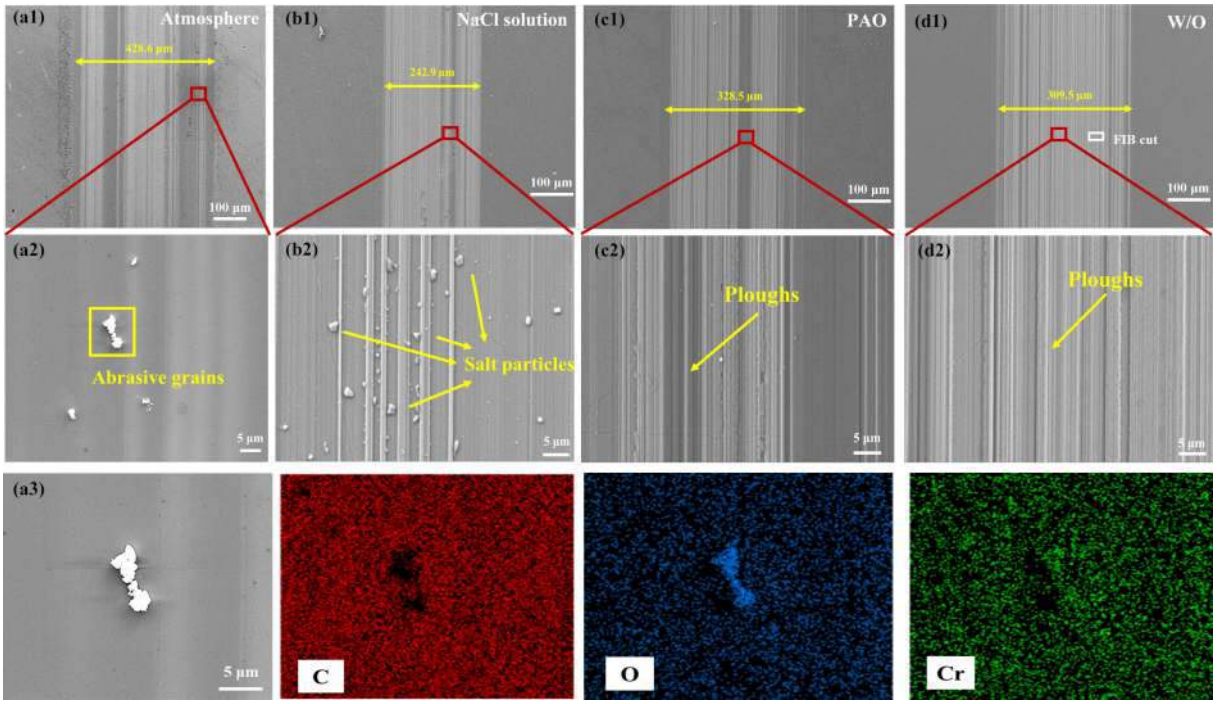

Fig. 9 SEM images and EDS maps of wear tracks of Cr/a-C:Cr coatings under (a) atmospheric, (b) NaCl solution, (c) PAO oil, and (d) W/O conditions.

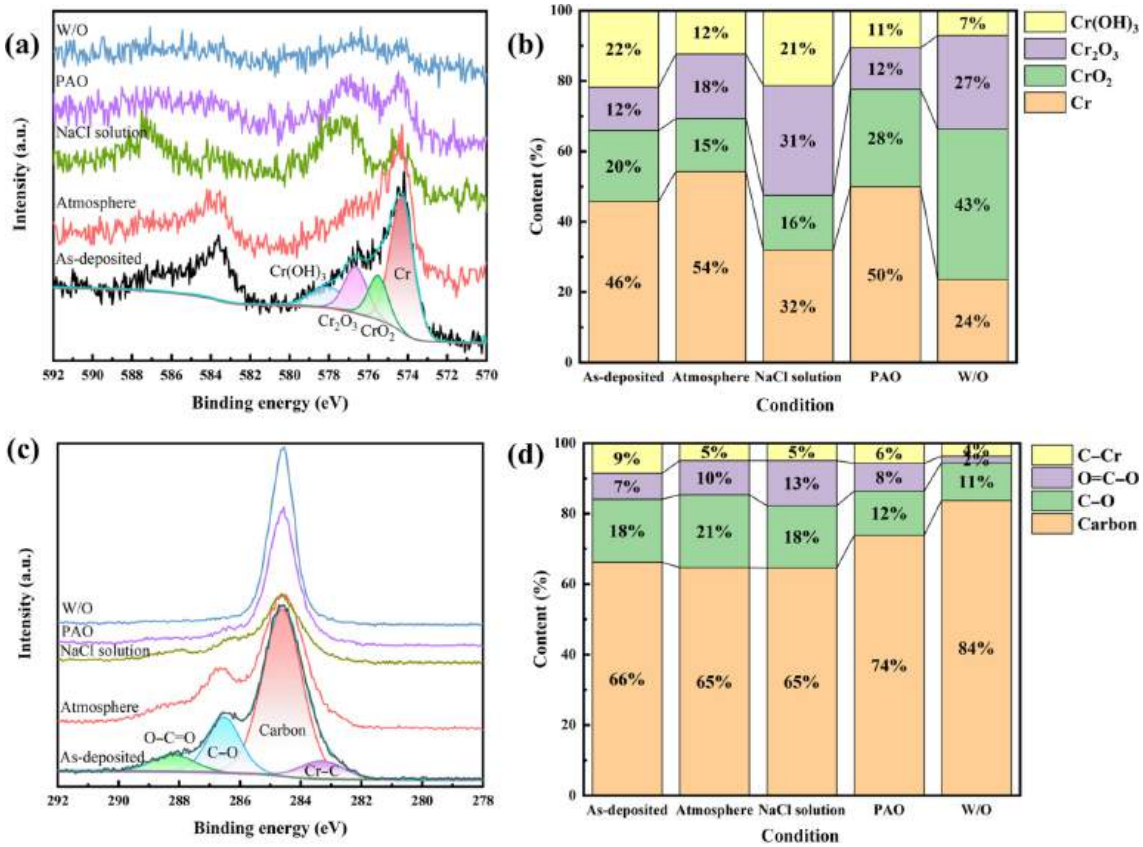

Fig. 10 XPS spectra of (a, b) Cr 2p and (c, d) C 1s of Cr/a-C:Cr coating under different conditions.

resistance, followed by the W/O condition (Fig. 6(a)). Since the outermost a-C layer had high chemical inertness, the formed transfer film and liquid characteristics determine the tribological behavior. Due to the good lipophilicity of PEEK (Fig. 3) and the high kinematic viscosity of PAO, PAO oil films can be formed on the PEEK surface, which can separate PEEK from the Cr/a-C coating, and the pair shows low shear lubrication properties [37]. In addition, upon the addition of a 9.1 wt% NaCl solution to PAO oil, the molecular chain might be dissociated, increasing the energy loss inside the light oil and resulting in an increase in the friction coefficient of the system [38, 39].

For the Cr/a-C:Cr coating with a PEEK counterbody, the metal

oxidation effect was remarkable, and the formed Cr_2O_3 nanocrystals can cause severe abrasive wear. Under atmospheric conditions (Fig. 5(b)), the COF decreased significantly and stabilized at ~0.2. The doping of Cr significantly reduced the wear of PEEK but enhanced the wear rate of the coating, as shown in Fig. 6. The surface morphology and Raman spectra of the wear scars showed that graphitized transfer films were formed (Figs. 7 and 8), suggesting that Cr promoted the formation of graphitization transfer films. The graphitized transfer film provided lubrication and reduced the wear of PEEK. Furthermore, under NaCl solution conditions, the wear rate of the coating was still high, and the COF of the pair and the PEEK wear volume decreased significantly. This was the result of the synergistic effect of the graphitized transfer film and liquid lubrication.

Under PAO oil and W/O conditions, an oil film formed on the surface of the PEEK ball due to the oleophilic properties of PEEK (Fig. 3), which hindered the adhesion of the graphitized transfer film (Fig. 7). However, the oil film can separate the friction contact surface and form fluid lubrication, so that the Cr/a-C:Cr and PEEK pair also showed excellent wear resistance [40]. SEM images of the wear track revealed that the coating experienced severe abrasive wear, especially under W/O conditions (Fig. 9). EDS analysis revealed the accumulation of O and Cr in the wear particles, as shown in Fig. 9(a3). The XPS results of the wear track showed that a large amount of Cr oxides formed on the coating surface under W/O conditions (Fig. 10). TEM analysis of the wear track indicated that Cr_2O_3 nanocrystals were present near the surface (Fig. 11). This proved that hard particles of chromium oxide formed after the Cr/a-C:Cr coating slid under W/O conditions. Compared to that of PAO oil, the stability of the W/O emulsion is poor, which is due to droplet size variation and migration of water [41]. This unstable lubrication environment may accelerate the oxidation of Cr, resulting in more severe abrasive wear. Figure 12 shows the mechanism diagram of the tribological behavior of the Cr/a-C:Cr coating against PEEK under different conditions.

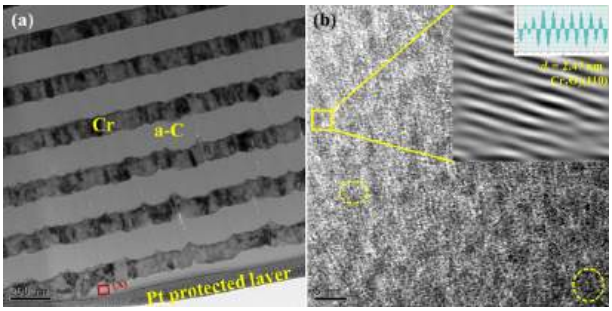

Fig. 11 (a) Cross-sectional TEM images of wear track on Cr/a-C:Cr coating under W/O conditions and (b) corresponding HRTEM image of near surface (position A in (a)).

5 Conclusions

In conclusion, in view of the wear failure of dynamic seal components for some marine engineering equipment, NaCl solution, PAO oil, and W/O were used as lubricants to systematically study the tribological behavior of PEEK and a-C-coated stainless steel pairs. Under atmospheric conditions and in a NaCl solution, the introduction of Cr at the top layer facilitated the formation of an a-C-containing transfer film, resulting in a low and stable COF. Among these, the enhancement was most pronounced under atmospheric conditions, resulting in a decrease in the COF from approximately 0.4 to approximately 0.2. Conversely, in the PAO environment, the formation of the PAO oil film promoted fluid lubrication, although it prevented the formation of the transfer film, and the oil film played a dominant role at this time. However, in the W/O environment, due to the Cr activity and inherent instability of the W/O mixture, the emergence of a robust chrome oxide phase accelerated, thereby intensifying the abrasion phenomenon. Therefore, Cr-doped modified a-C coatings were not suitable for all lubrication environments. Evidently, in practical scenarios, different from the viscosity of lubricant oil, it is imperative to consider the interaction between the coating and corrosive environments with oxygen or Cl, since possible tribo-chemical reactions can also change the tribological interface characteristics.

It is imperative to acknowledge that the composite friction characteristics of the three solid lubricants, namely, metal oxides, a-C, and PEEK, exhibit significant variations when subjected to different solutions, and in certain cases, they may even manifest counterproductive outcomes. The judicious selection of frictional pairings under solid-liquid lubrication conditions is crucial for optimizing the efficiency of lubricating materials.

Acknowledgements

This work was financially supported by the National Key R&D Program of China (2022YFC2805701), the National Natural Science Foundation of China (52025014 and U20A20296),

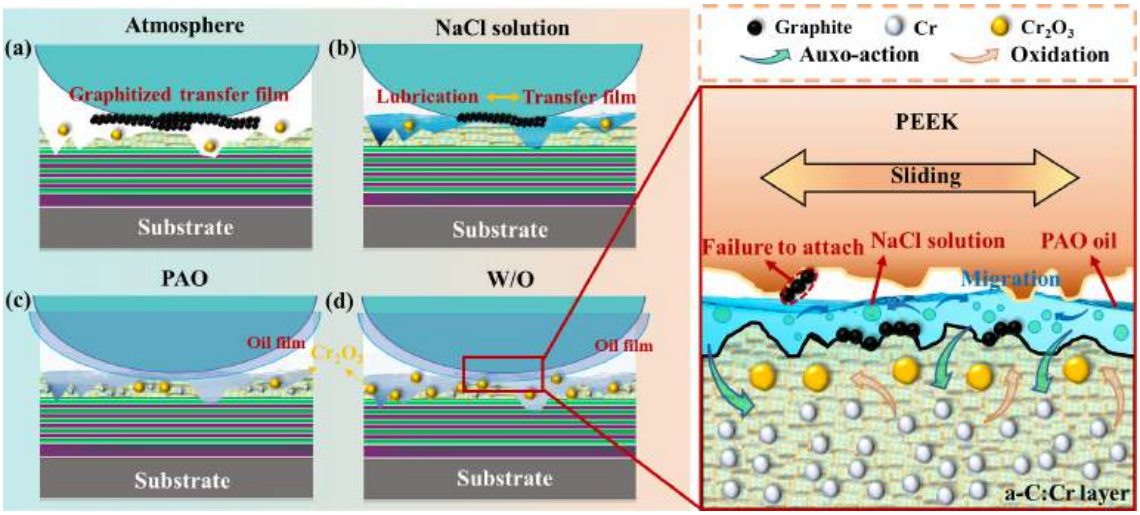

Fig. 12 Mechanistic diagram of tribological behavior of Cr/a-C:Cr coating against PEEK under (a) atmospheric, (b) NaCl solution, (c) PAO, and (d) W/O conditions.

Zhejiang Lingyan Research and Development Program (2024C01159), and Major Special Project of Ningbo (2023Z198).

CRediT authorship contribution statement

Xiaohui Zhou: methodology, investigation, validation, and writing original draft; Yingpeng Zhang: methodology and investigation; Hao Li: methodology and investigation; Li Cui: visualization; Aiying Wang: writing–review & editing, funding acquisition, and supervision; Peng Guo: writing–review & editing, methodology, and supervision; Peiling Ke: writing–review & editing, supervision, and funding acquisition.

Declaration of competing interest

The authors have no competing interests to declare that are relevant to the content of this article.

Electronic Supplementary Material

Supplementary material is available in the online version of this article at https://doi.org/10.26599/FRICT.2025.9440920.

References

[1] Zhang C, Chen R T, Bai G H, Wang S P, Tomovic M M. Reliability estimation of rotary lip seal in aircraft utility system based on time-varying dependence degradation model and its experimental validation. *Chin J Aeronaut* **33**(8): 2230–2241 (2020)

[2] Wang H J, Gao Z Q, He X Z, Li Z K, Zhao J Q, Luo Z, Wei Y Q. Performance of magnetic fluid and back blade combined seal for sealing water. *Magnetochemistry* **9**(2): 38 (2023)

[3] Wang Z Q, Gao D R. Comparative investigation on the tribological behavior of reinforced plastic composite under natural seawater lubrication. *Mater Des* **51**: 983–988 (2013)

[4] Wang Z Q, Ni J, Gao D R. Combined effect of the use of carbon fiber and seawater and the molecular structure on the tribological behavior of polymer materials. *Friction* **6**(2): 183–194 (2018)

[5] Fu J, Lyu D C, Kang J, Li Y C, Zhao J G. Tribological characteristics of hard-to-hard matching materials of cylinder block/valve plate interface in electro-hydrostatic actuator pumps. *P I Mech Eng C—J Mec* **238**(6): 2393–2406 (2024)

[6] Traverso P, Canepa E. A review of studies on corrosion of metals and alloys in deep-sea environment. *Ocean Eng* **87**: 10–15 (2014)

[7] Ayala H M, Hart D P, Yeh O C, Boyce M C. Wear of elastomeric seals in abrasive slurries. *Wear* **220**(1): 9–21 (1998)

[8] Gong R, Wang H, Zhang H, Xu Y. Influence of wear on hot banding migration of sealing ring using FEM. *Wear* **428**: 449–456 (2019)

[9] Lettington AH. Applications diamond-like carbon thin films. *Carbon* **36**(5–6): 555–560 (1998).

[10] Al-Azizi A A, Eryilmaz O, Erdemir A, Kim S H. Nano-texture for a wear-resistant and near-frictionless diamond-like carbon. *Carbon* **73**: 403–412 (2014)

[11] Marino M J, Hsiao E, Chen Y S, Eryilmaz O L, Erdemir A, Kim S H. Understanding run-in behavior of diamond-like carbon friction and preventing diamond-like carbon wear in humid air. *Langmuir* **27**(20): 12702–12708 (2011)

[12] Liu Y R, Du H, Zuo X, Guo P, Liu L, Lee K R, Wang A Y, Ke P L. Cr/GLC multilayered coating in simulated deep-sea environment: Corrosion behavior and growth defect evolution. *Corros Sci* **188**: 109528 (2021)

[13] Jacobs O, Jaskulka R, Yan C, Wu W. On the effect of counterface material and aqueous environment on the sliding wear of carbon fibre reinforced polyetheretherketone (PEEK). *Tribol Lett* **19**(4): 319–329 (2005)

[14] Franta L, Fojt J, Joska L, Kronek J, Cvrcek L, Vyskocil J, Cejka Z. Hinge-type knee prosthesis wear tests with a mechanical load and corrosion properties monitoring. *Tribol Int* **63**: 61–65 (2013)

[15] Patnaik L, Maity S R, Kumar S. Effect of lubricated sliding wear against CFRPEEK on the nanomechanical properties of Ag alloyed Cr/DLC thin film. *J Mech Behav Biomed Mater* **118**: 104478 (2021)

[16] Escudeiro A, Wimmer M A, Polcar T, Cavaleiro A. Tribological behavior of uncoated and DLC-coated CoCr and Ti-alloys in contact with UHMWPE and PEEK counterbodies. *Tribol Int* **89**: 97–104 (2015)

[17] Zhou X H, Zhang Y P, Guo P, Cui L, Wang A Y, Ke P L. Tribological behavior of Cr/a-C multilayered coating against PEEK under dry sliding condition. *Wear* **518–519**: 204625 (2023)

[18] Amanov A, Watabe T, Tsuboi R, Sasaki S. Fretting wear and fracture behaviors of Cr-doped and non-doped DLC films deposited on Ti–6Al–4V alloy by unbalanced magnetron sputtering. *Tribol Int* **62**: 49–57 (2013)

[19] Santiago J A, Fernández-Martínez I, Sánchez-López J C, Rojas T C, Wennberg A, Bellido-González V, Molina-Aldareguia J M, Monclús M A, González-Arrabal R. Tribomechanical properties of hard Cr-doped DLC coatings deposited by low-frequency HiPIMS. *Surf Coat Technol* **382**: 124899 (2020)

[20] Li L, Liu L L, Li X W, Guo P, Ke P L, Wang A Y. Enhanced tribocorrosion performance of Cr/GLC multilayered films for marine protective application. *ACS Appl Mater Inter* **10**(15): 13187–13198 (2018)

[21] Li H, Liu L L, Guo P, Sun L L, Wei J, Liu Y R, Li S Y, Wang S Y, Lee K R, Ke P L, et al. Long-term tribocorrosion resistance and failure tolerance of multilayer carbon-based coatings. *Friction* **10**(10): 1707–1721 (2022)

[22] Ghaednia H, Pope S A, Jackson R L, Marghitu D B. A comprehensive study of the elasto-plastic contact of a sphere and a flat. *Tribol Int* **93**: 78–90 (2016)

[23] Kalin M, Polajnar M. The correlation between the surface energy, the contact angle and the spreading parameter, and their relevance for the wetting behaviour of DLC with lubricating oils. *Tribol Int* **66**: 225–233 (2013)

[24] Chen J, Cai W J. Effect of scratching frequency on the tribocorrosion resistance of Al–Mn amorphous thin films. *Wear* **426**: 1457–1465 (2019)

[25] Li L, Guo P, Liu L L, Li X W, Ke P L, Wang A Y. Structural design of Cr/GLC films for high tribological performance in artificial seawater: Cr/GLC ratio and multilayer structure. *J Mater Sci Technol* **34**(8): 1273–1280 (2018)

[26] Pawlak Z, Urbaniak W, Oloyede A. The relationship between friction and wettability in aqueous environment. *Wear* **271**(9–10): 1745–1749 (2011)

[27] Dyson HJ, Wright PE, Scheraga HA. The role of hydrophobic interactions in initiation and propagation of protein folding. *Proc Natl Acad Sci USA* **103**(35): 13057–13061 (2006)

[28] Ma C D, Wang C X, Acevedo-Vélez C, Gellman S H, Abbott N L. Modulation of hydrophobic interactions by proximally immobilized ions. *Nature* **517**(7534): 347–350 (2015)

[29] Wang A Y, Lee K R, Ahn J P, Han J H. Structure and mechanical properties of W incorporated diamond-like carbon films prepared by a hybrid ion beam deposition technique. *Carbon* **44**(9): 1826–1832 (2006)

[30] Casiraghi C, Ferrari A C, Robertson J. Raman spectroscopy of hydrogenated amorphous carbons. *Phys Rev B* **72**(8): 085401 (2005)

[31] Prawer S, Nugent K W, Lifshitz Y, Lempert G D, Grossman E, Kulik J, Avigal I, Kalish R. Systematic variation of the Raman spectra of DLC films as a function of sp^2:sp^3 composition. *Diam Relat Mater* **5**

(3–5): 433–438 (1996)
[32] Schwan J, Ulrich S, Batori V, Ehrhardt H, Silva S R P. Raman spectroscopy on amorphous carbon films. *J Appl Phys* **80**(1): 440–447 (1996)
[33] Ouchabane M, Dublanche-Tixier C, Dergham D. Nanoindentation data analysis of loading curve performed on DLC thin films: Effect of residual stress on the elasto-plastic properties. *J Appl Phys* **122**(17): 175103 (2017)
[34] Kubo Y, Sonohara Y, Uemura S. Changes in the chemical state of metallic Cr during deposition on a polyimide substrate: Full soft XPS and ToF–SIMS depth profiles. *Appl Surf Sci* **553**: 149437 (2021)
[35] Ishitani A. Application of X-ray of photoelectron spectroscopy to surface analysis of carbon fiber. *Carbon* **19**(4): 269–275 (1981).
[36] Pal SK, Jiang J, Meletis EI. Effects of N-doping on the microstructure, mechanical and tribological behavior of Cr-DLC films. *Surf Coat Tech* **201**(18): 7917–7923 (2007).
[37] Du N Z, Wei X B, Li X W, Chen Z, Lu S Q, Ding J Q, Feng C N, Chen K, Qiao J H, Zhang D K, et al. Friction reactions induced by selective hydrogenation of textured surface under lubricant conditions. *Friction* **12**(1): 174–184 (2024)
[38] Liu Y H, Zhang H, Liu T, Wang X W, Luo Y Y, Zhu X H. Exploring the effects of water content on friction behavior and mechanism of DLC films in oil production environment based on molecular dynamics simulation and first-principles calculations. *Diam Relat Mater* **139**: 110294 (2023)
[39] Zhao S Y, Xu C G, Zhang J X, Liang Y M, Liu W M, Huang J X, Guo Z G. A robust membrane with dual superlyophobicity for solving water-caused lubricant deterioration and water contamination. *Friction* **11**(8): 1442–1454 (2023)
[40] Guo Y Z, Guo P, Sun L L, Li X W, Ke P L, Li Q, Wang A Y. Tribological properties of Ti-doped diamond-like carbon coatings under dry friction and PAO oil lubrication. *Surf Interface Anal* **51**(3): 361–370 (2019)
[41] Xu B, Kang W, Wang X, Meng L. Influence of water content and temperature on stability of W/O crude oil emulsion. *Petrol Sci Technol* **31**(10): 1099–1108 (2013)

Xiaohui Zhou received her B.S. degree in material physics from China University of Petroleum, China. She is now a joint Ph.D. candidate at Shanghaitech University, China and Ningbo Institute of Materials Technology and Engineering, Chinese Academy of Sciences, China. Her research includes the design and preparation of carbon-based coatings and the study of friction failure behavior in harsh environments.

Peng Guo received his Ph.D. degree from the University of Chinese Academy of Sciences, China, in July 2015. He is currently an associate professor at the Ningbo Institute of Materials Technology and Engineering, Chinese Academy of Sciences, China. His research interests include the preparation and characterization of amorphous carbon films as well as the application of related functional devices.

Peiling Ke received her Ph.D. degree from the Institute of Metal Research, Chinese Academy of Sciences (CAS), China, in 2006 and was assigned to the University of Birmingham, UK. After graduation, she served as a visiting research fellow at the University of Birmingham. Since 2009, she started working at the Ningbo Institute of Materials Technology and Engineering (NIMTE), CAS, China, and was a professor in 2015. She is currently the director of the Public Technology Center of NIMTE. Her research has focused mainly on the use of protective coating materials for marine applications and related evaluation methodologies.